Brain Structure and Function (2019) 224:3247–3262
https://doi.org/10.1007/s00429-019-01971-0

ORIGINAL ARTICLE

Non-radial tortuous migration with cell polarity alterations of newly generated granule neurons in the neonatal rat dentate gyrus

Takashi Namba[1,2,4] · **Hiroshi Shinohara**[3] · **Tatsunori Seki**[1,3]

Received: 22 February 2019 / Accepted: 17 October 2019 / Published online: 28 October 2019

Abstract

To establish functional neuronal circuits, newborn neurons generally migrate from the ventricular germinal zones to their final positions during embryonic periods. However, most excitatory neurons of the hippocampal dentate gyrus are born postnatally in the hilus, far from the lateral ventricle. Newly generated granule neurons must then migrate to the surrounding granule cell layer (GCL), which suggests that newborn granule cells may migrate by unique cellular mechanisms. In the present study, we describe the migratory behaviors of postnatally generated granule neurons using combined retroviral labeling and time-lapse imaging analysis. Our results show that whereas half of the newly generated neurons undergo radial migration, the remainder engages in more complex migratory patterns with veering and turning movements accompanied by process formation and cell polarity alterations. These data reveal a previously unappreciated diversity of mechanisms by which granule neurons distribute throughout the GCL to contribute to hippocampal circuitry.

Keywords Hippocampus · Neurogenesis · Migration · Slice culture · Time-lapse imaging · Neuronal polarity

Introduction

Proper neuronal migration is critical for the establishment of functional neuronal circuits during brain development. Because neurons are generally produced either in the ventricular zone (VZ) or the subventricular zone (SVZ) surrounding the ventricle, they must sometimes travel considerable distances to reach their final destinations in the mantle layer. The cellular and molecular mechanisms governing the migration of newborn neurons to appropriate locations are active areas of research with clear implications for human health (Kerjan and Gleeson 2007; Reiner and Sapir 2013; Stouffer et al. 2016). It is known, for example, that disruptions to neuronal migration in the developing human cerebral cortex can lead to severe neurodevelopmental disorders including lissencephaly (Kerjan and Gleeson 2007; Reiner and Sapir 2013; Stouffer et al. 2016).

The dentate gyrus (DG) forms the medial part of the hippocampus, a highly conserved center of memory and learning in mammals (Abrous and Wojtowicz 2015; Josselyn et al. 2015; Moser et al. 2017; Nakazawa et al. 2004). There are mainly three germinal zones for development of the hippocampal granule cells (Supplementary Fig. 1) (Altman and Bayer 1990a, b; Hevner 2016; Li and Pleasure 2014; Namba et al. 2005; Seki et al. 2014). The primary germinal zone (until E20) is the VZ and SVZ of the pallial neuroepithelium (Altman and Bayer 1990a; Nicola et al. 2015; Seki et al. 2014). The progenitor cells in the VZ and SVZ generate excitatory neurons that finally populate less than 20% of the granule cell layer (GCL) in the DG and majority of the pyramidal cell layer in Ammon's horn, the two principal subdivisions of the adult hippocampus (Bayer 1980).

Electronic supplementary material The online version of this article (https://doi.org/10.1007/s00429-019-01971-0) contains supplementary material, which is available to authorized users.

✉ Takashi Namba
namba-takashi@suou.waseda.jp

✉ Tatsunori Seki
sekit@tokyo-med.ac.jp

[1] Department of Anatomy, Juntendo University School of Medicine, Tokyo 113-8421, Japan

[2] Integrative Bioscience and Biomedical Engineering, School of Science and Engineering, Waseda University, Tokyo 169-8555, Japan

[3] Department of Histology and Neuroanatomy, Tokyo Medical University, Tokyo 160-8421, Japan

[4] Present Address: Max Planck Institute of Molecular Cell Biology and Genetics, Dresden, Germany

The secondary germinal zone, so called the dentate migratory stream, consists of the progenitor cells migrating away from the VZ and SVZ toward the emerging dentate gyrus while maintaining proliferative activity (Supplementary Fig. 1) (Altman and Bayer 1990a; Nicola et al. 2015; Seki et al. 2014). During the perinatal period (embryonic day 20 (E20)—postnatal day 3 (P3) in rat), the progenitor cells in the dentate migratory stream develop approximately 40% of GCL (Bayer 1980).

Thereafter the progenitor cells migrate and form the tertiary germinal zone in the hilus until P3 to P5 (Supplementary Fig. 1) (Altman and Bayer 1990a, b; Namba et al. 2005; Nowakowski and Rakic 1981; Rakic and Nowakowski 1981; Schlessinger et al. 1975; Seki et al. 2014). The rest of GCL (approximately 40%) are generated from the progenitor cells in the hilus during P3 to P10.

As the development of GCL proceeds, the tertiary germinal zone in the hilus gradually shrinks until P19 and finally forms the subgranular zone (SGZ), the adult neurogenic niche (Supplementary Fig. 1). The progenitor cells in the adult SGZ continuously generate neurons throughout life and are thought to be involved in the hippocampal function (Altman and Das 1965; Eriksson et al. 1998; Kempermann 2019; Kuhn et al. 1996; Seki and Arai 1993, 1995; Toda and Gage 2018).

Neonatal neurogenesis in the hilus is crucial for the formation of hippocampal circuitry. For example, peak neurogenesis of granule cells coincides with the initial formation of connections between granule cells and the CA3 pyramidal cells in Ammon's horn (Amaral and Dent 1981; Blaabjerg and Zimmer 2007). Despite the importance of postnatal hilar neurogenesis (Bayer and Altman 1975), the mechanisms by which postnatally generated granule neurons reach their proper locations in the GCL remain incompletely understood. Previous immunohistochemical studies suggest that a majority of the immature granule neurons in the neonatal rodent hilus migrate radially (Nakahira and Yuasa 2005; Sievers et al. 1992). These observations are corroborated by a time-lapse imaging analysis of the migrating neurons in the neonatal rat hilus (Koyama et al. 2012). However, two other studies showed the existence of the non-radial (tangential) migration in the neonatal rodent hilus by time-lapse imaging (Seki et al. 2007; Wang et al. 2018).

In this study, we focused on the immature granule neurons within the hilus at P8, which are the progeny of the progenitor cells of the tertiary germinal zone, and their migratory behaviors in transit to the GCL. Consistent with previous studies in the developing neocortex and other structures, we found that half of the migrating cells exhibited conventional radial migration. However, we also observed abundant populations of migrating granule cells that traveled through complex, tangential routes and which made frequent directional changes through alterations to their cellular polarities. We suggest that these tangential migratory patterns may serve to distribute granule neurons evenly throughout the U-shaped structure of the dentate gyrus.

Materials and methods

Animals

All animal experiments were approved by the institutional animal care and use committee at Juntendo University and Tokyo Medical University. All Wister rats used in this study were purchased from CLEA Japan. For immunohistochemical analysis, total 9 (P8) and 3 (P19) rats were used. For time-lapse imaging analysis, total 10 rats were used.

Retroviral injections

To visualize migrating neurons, we used the GCDNsap-EGFP retrovirus vector (Suzuki et al. 2002). Postnatal day 5 (P5) rats were anaesthetized on ice and stereotactically injected with 0.5 µl of retrovirus vector into the DG of the hippocampus (anteroposterior, 1.2 mm from bregma; lateral, 2.1 mm; ventral, 2 mm), as described previously (Namba et al. 2005). At 3 (P8) or 14 (P19) days following the retroviral injection, rats were perfused with fixative or processed for the time-lapse imaging analysis as described below.

Immunohistochemistry

P8 and P19 Wistar rats were deeply anaesthetized with sodium pentobarbital, and perfused intracardially with 0.01 M phosphate-buffed saline (PBS), pH 7.4, followed by 4% paraformaldehyde (for GABA staining, glutaraldehyde was added to obtain the final concentration at 0.1%) in 0.1 M phosphate buffer (PB), pH 7.4, at room temperature. The brains were postfixed in the same fixative overnight at 4 °C. The fixed brains were washed with PBS and immersed in 10% and then 20% sucrose in PBS overnight at 4 °C. The hippocampal formation was then dissected from the remaining brain structure, embedded in OTC compound, and placed at − 80 °C for a long-term storage. The samples were thawed, washed with PBS, and embedded in 5% agarose in PBS. The hippocampi were sectioned in a plane perpendicular to the septo-temporal axis of the hippocampal formation by a vibratome into sections 50-µm thick, as described previously (Namba et al. 2005). Hippocampal formations from the region within approximately ± 1 mm from the injection site were sectioned. This region represents the middle of the dorsal hippocampus. There was no obvious tissue damage

after freeze-and-thaw of the hippocampi compared to the hippocampi without frozen.

Hippocampal sections were incubated overnight with primary antibody mixtures containing 1% BSA and 1% normal donkey serum at 4 °C. We used the following primary antibodies: rabbit anti-calretinin (1:2000, 7669/4, Swant, Switzerland), rabbit anti-GABA (1:2000, A2052, Sigma MO), mouse anti-GFP (1:400, G6539, sigma), rabbit anti-GFP (1:1000, gift from Dr. Tamamaki at Kumamoto University), rat anti-GFP (1:500, 04404-26, Nacalai Tesque, Japan), human anti-Hu (1:2000, a neuronal marker, gift from Dr. Okano at The Jikei University School of Medicine), rabbit anti-Iba-1 (1:500, a microglia marker, 234-003, Synaptic Systems, Germany), rabbit anti-Prox1 (1:1000, a granule cell marker, AB5475, Chemicon, CA), rabbit anti-S100β (1:5000, an astrocyte marker, 37, Swant) and mouse anti-S100β (1:2000, S2532, Sigma). The sections were washed with PBS and incubated with the secondary antibodies as follows: donkey anti-mouse IgG-Cy2 and -Cy5 (1:200, 715-225-151 and 715-175-151, respectively, Jackson, PA), donkey anti-human IgG-Cy3 (1:200, 709-165-149, Jackson) and donkey anti-rabbit IgG-Cy2 and -Cy5 (1:200, 711-225-152 and 711-175-152, respectively, Jackson). After washing with PBS, the samples were mounted on glass slides and the entire DG was imaged using a confocal laser-scanning microscope (LSM510 META; Zeiss, Germany) with 20×, 40× and 100× objectives without digital zooming. Ten to sixty z-stacks of optical sections (4.2 µm for 20×-objective, 1.8 µm for 40×-objective and 0.7 µm for 100×-objective in thickness) were obtained at 2.1 µm increments in the *z*-axis for the 20×-objective, 0.9 µm for the 40×-objective and 0.4 µm for the 100×-objective analysis.

Quantification of GFP-labeled cells

To quantify the percentage of GFP+ cells that are GABA+, Hu+, Prox1+ and/or S100β+, 42–192 cells per experiments were counted.

To quantify the morphotypes of GFP+ Hu+ or GFP+Hu+Prox1+ cells in the hilus, we analyzed the images taken by the confocal laser-scanning microscope with ZEN (Zeiss) software. We excluded clustered GFP+ cells as well as single GFP+ cells with faint GFP expression from the quantification because the determination of morphotypes of these cells was difficult. For this quantification, approximately 10–20 cells per sections were counted.

To analyze the orientation of GFP+Hu+ cells, we measured the angle between the direction to the nearest GCL and the leading process by Fiji. Because the middle of the dorsal hippocampus was sectioned in a plane perpendicular to the septo-temporal axis, we could analyze the orientation in a 2D plane.

Slice culture and time-lapse imaging

Slice culture preparation and time-lapse imaging were performed as described previously (Namba et al. 2011b). Three days after retroviral injection (P8), rats were deeply anaesthetized with diethyl ether. Hippocampal formations from the region within approximately ± 1 mm from the injection site were sectioned at 350 µm thickness in a plane perpendicular to the septo-temporal axis of the hippocampal formation and transferred onto a collagen-coated glass bottom dish (35 mm in diameter, WillCo Wells, The Netherlands). Slices with damage caused by the injection were excluded from the analysis. The slices were kept in a mixture of 50% MEM (Invitrogen), 25% heat inactivated horse serum (Invitrogen), and 25% Hank's balanced salt solution (Invitrogen) supplemented with penicillin–streptomycin–glutamine (Invitrogen) and glucose at a final concentration of 6.5 mg/mL. Time-lapse imaging was performed 20–24 h using an inverted confocal laser-scanning microscope (LSM510 META) with minimal laser excitation (typically 1% of an Argon 488 laser) to avoid photodamage and photobleaching. To track the movements of the GFP-labeled cells, Z-stacks of 20–30 optical sections (1.8 µm in thickness per optical section) were collected every 2 h using a 20× objective. During the interval of imaging, the slices were kept in a water-jacketed incubator at 37 °C and 5% CO_2 as described previously (Noctor et al. 2001). Z-stack images at each time point were created and analyzed using LSM image Browser (Zeiss), ZEN (Zeiss) and Photoshop (Adobe Systems, CA). The distance of cell migration was analyzed by Fiji.

Statistical analysis

Data were analyzed with Excel (Microsoft, WA), Statcel3 (OMS, Japan) and MYSTAT (Systat Software, CA). Statistical tests: for two groups of observations that do not follow a normal distribution, the Mann–Whitney *U*-test was used. For the normality test, the Shapiro–Wilk normality test was used. All values are given as mean ± SEM. The values in Fig. 6 are given as mean.

Results

Morphology and migration directionality of newly generated neurons in vivo

The direction of movement of migrating cells can be predicted by the morphology and orientation of their neuronal processes in the embryonic neocortex (Kawauchi 2015; Nadarajah et al. 2003; Namba et al. 2015; Reiner and Sapir 2013). We, therefore, examined the localization, morphology

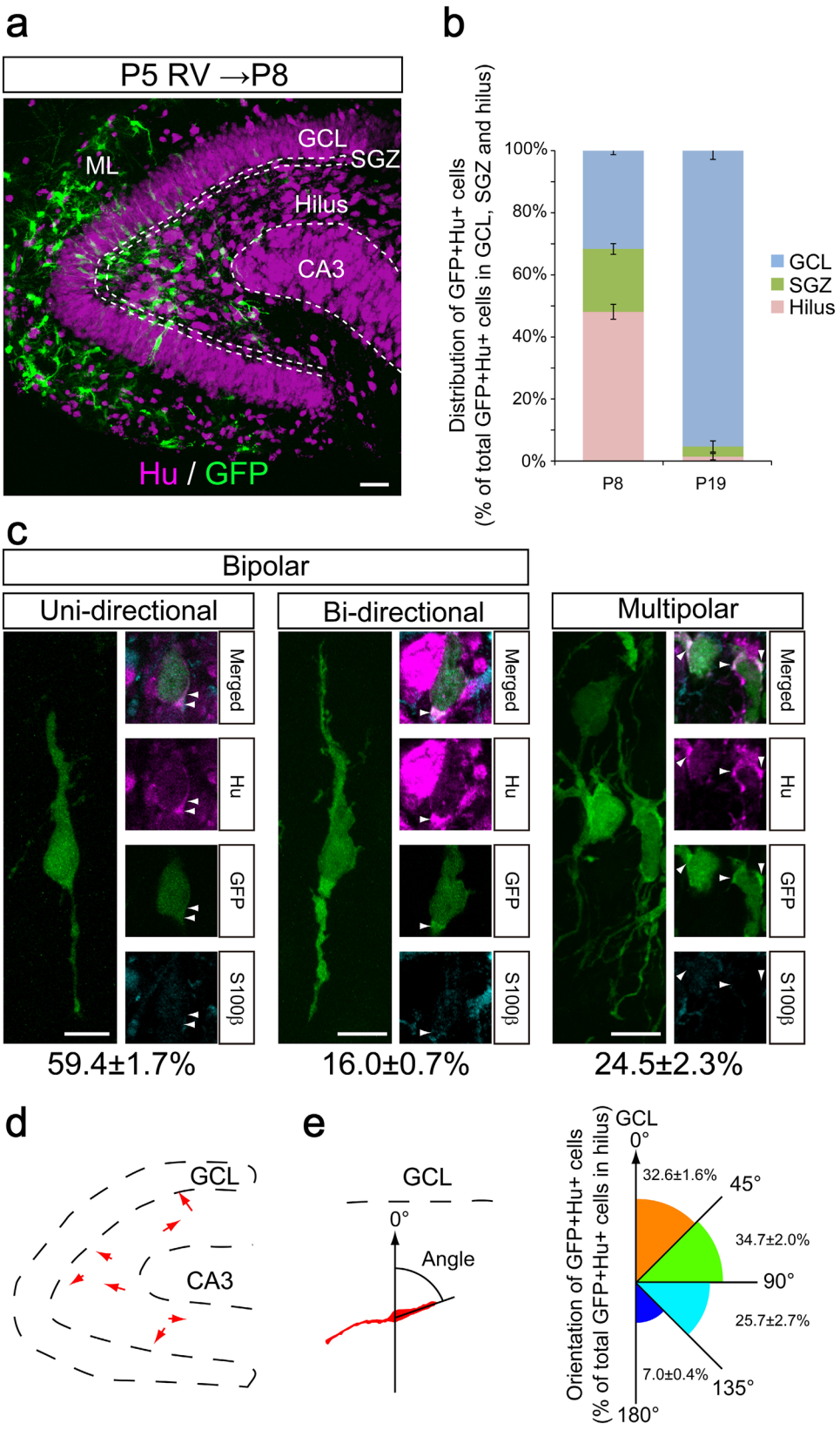

Fig. 1 Distribution and morphotypes of GFP+ neurons in the postnatal DG. Retrovirus carrying GFP was injected into DG to label the progenitor cells and their progenies at P5 and analyzed at P8. **a** GFP (green) and Hu (magenta) double immunofluorescence in the rat DG at P8. Dashed lines indicate the boundaries between GCL, SGZ, hilus and CA3. Scale bar, 50 µm. **b** Quantification of the percentage of GFP+Hu+ cells that are localized in the GCL (blue) and hilus (pink) at P8. Error bar indicates S.E.M. **c** GFP (green), Hu (magenta) and S100β (cyan) triple immunofluorescence of cells located in the P8 rat hilus. The percentage of each morphotypes in the GFP+Hu+ hilus cells are shown on the bottom of each sub-panels. Scale bars, 10 µm. Arrowheads indicate the GFP+ cytoplasm positive for Hu. Total 151 GFP+Hu+ cells from three rats (3–6 sections per animal) were analyzed. **d** Distribution of uni-directional bipolar GFP+Hu+ cells in the rat hilus at P8. Arrows represent the localization of the GFP+Hu+ cells and also indicate the orientation of processes. **e** The angle between the direction of the nearest GCL (dashed line, left) and the leading process of uni-directional bipolar GFP+Hu+ cells (red, left). The angle is categorized into four groups; 0°–45°, 45°–90°, 90°–135°, 135°–180° (right). Area of sectors indicate the relative value of the percentage. Total 43 GFP+Hu+ cells from three rats (3–6 sections per animal) were analyzed

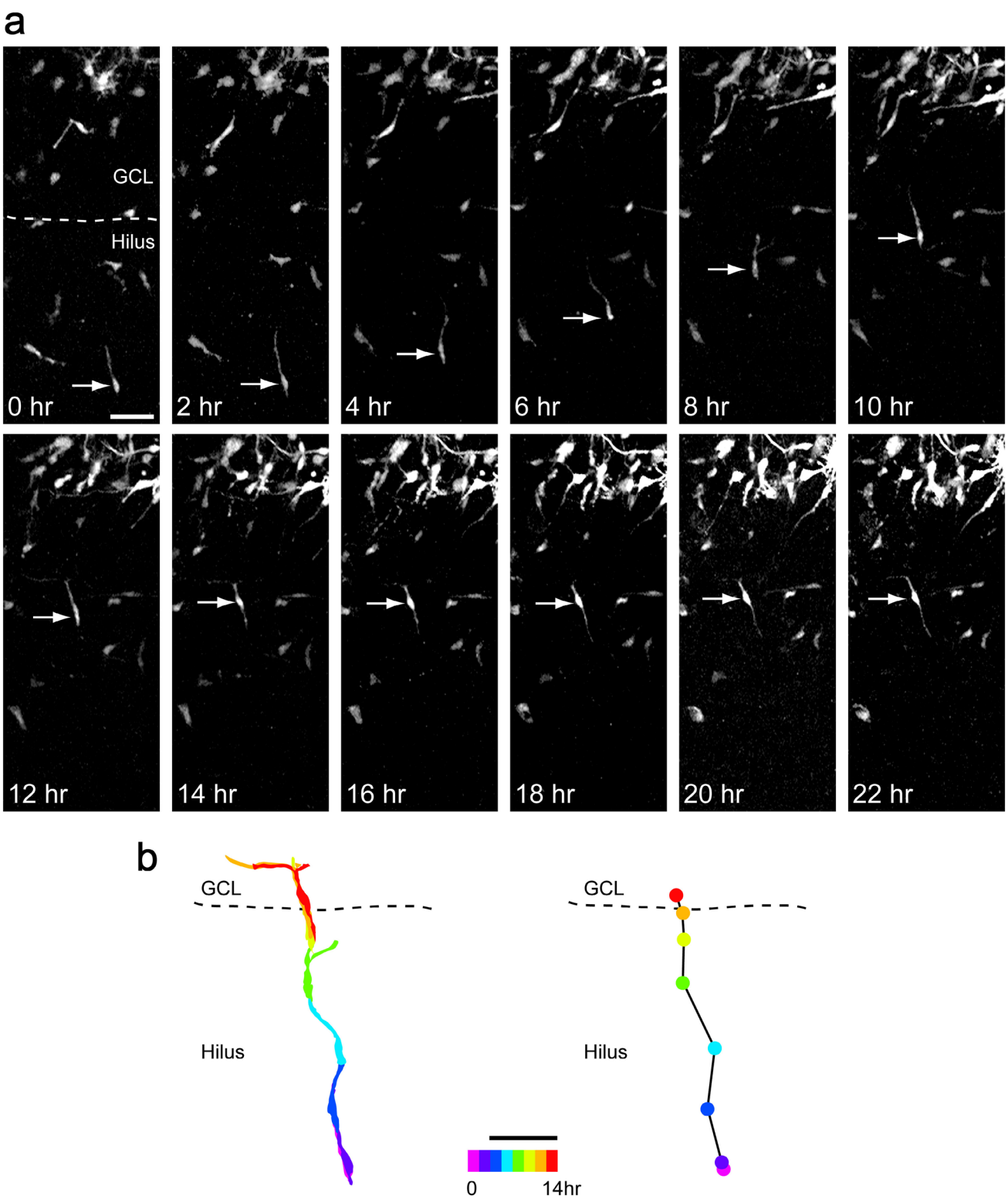

Fig. 2 Time-lapse images of radial migration of a GFP+cell (arrows) that migrated in the range between 45° and −45° from the initial direction (0°). Retrovirus carrying GFP was injected into at P5. Time-lapse imaging was started at P8. Images were taken every 2 h. **a** Panels show still images of GFP+cells. **b** Trajectory of the cell (left) and the position of cell soma (right) over time. Black line in the right panel shows the trajectory of soma. Each time-point is color-coded in the bottom of the panel. Scale bars, 50 µm

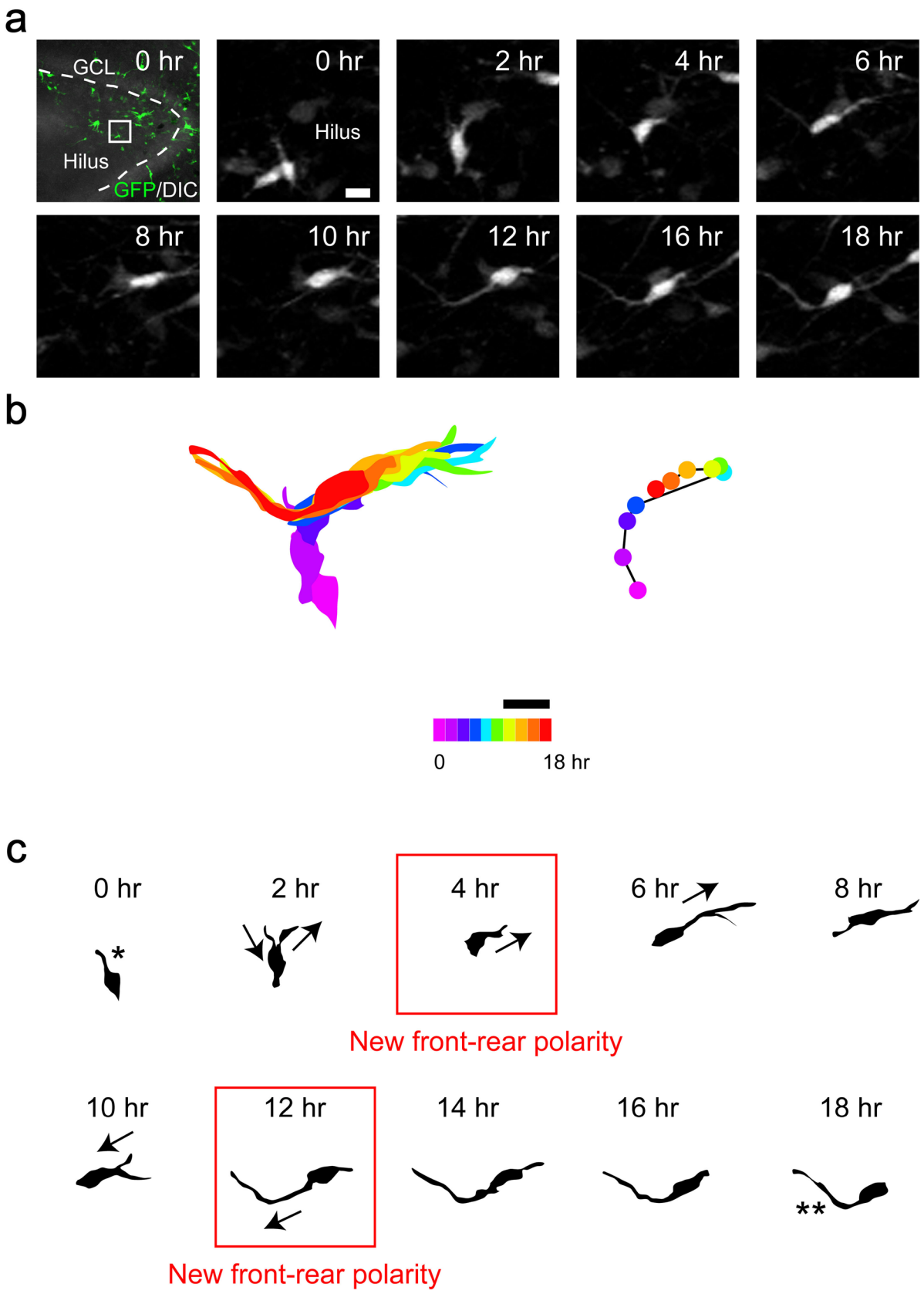
a
GCL
0 hr
Hilus
GFP/DIC
0 hr
Hilus
2 hr
4 hr
6 hr
8 hr
10 hr
12 hr
16 hr
18 hr
b
0
18 hr
c
0 hr
2 hr
4 hr
6 hr
8 hr
New front-rear polarity
10 hr
12 hr
14 hr
16 hr
18 hr
New front-rear polarity

◂**Fig. 3** Time-lapse images of veering and turning the movement of a GFP+ cell that showed new neurite formation from the soma during the migration. Retrovirus carrying GFP was injected into DG at P5. Time-lapse imaging was started at P8. Images were taken every 2 h. **a** Still images of GFP+ cells that changed their direction during migration. Higher magnification image of the boxed area in the leftmost top panel (0 h) are shown in the second left image. Scale bar, 10 µm. **b**, **c** Outline of the cell indicated by arrows in (**a**). **b** Trajectory of the cell (left) and position of cell soma (right) over time. Black line in the right panel shows the trajectory of soma. Each time-point is color-coded in the bottom of the panel. Scale bar, 10 µm. **c** Morphological changes of the cell over time. Asterisk indicates the initial leading processes. Double asterisk indicates the new leading processes. Small arrows indicate the neurite extension and retraction. Red boxes indicate the time point in which the cell established new front–rear polarity

and directionality of retrovirally labeled cells in fixed hippocampal tissue. Retroviral vector carrying GFP was stereotaxically injected into the rat DG at P5. Brain sections were processed for immunohistochemical analysis at either 3 days (P8) or 14 days (P19) after the injection. This method preferentially labeled the progenitor cells and their progenies in the DG as described previously (Namba et al. 2005).

At P8, more than 60% of the GFP-labeled (GFP+) cells in the hilus, SGZ and GCL expressed the neuronal marker Hu (64.3% ± 0.43), but not the astroglial cell marker S100β, suggesting that these cells were immature neurons. The remaining 40% of GFP+ cells were positive for S100β or negative for both markers, suggesting that these cells were either progenitors or non-neuronal cells such as astrocytes (Namba et al. 2005). Approximately half of the GFP+Hu+ cells were localized in the hilus (Fig. 1a, b, 48.1% ± 2.4) and the other half of cells were located either in GCL or SGZ (Fig. 1a, b, 31.7% ± 1.3 or 20.2% ± 1.7, respectively). The GFP + cells located in the molecular layer (ML) were positive for S100β (Supplementary Fig. 2a), indicating that these cells are astrocytes.

At P19, more than 95% of GFP+Hu+ cells in the DG were located in the GCL (Fig. 1b) and possessed typical morphological features of granule cells such as a single primary apical dendrite with branches and a single mossy fiber axon (Supplementary Fig. 3) (Namba et al. 2005). The differences in the localization of GFP+Hu+ cells observed across P8 and P19 suggest that the GFP+Hu+ cells in the hilus at P8 are immature neurons that differentiate to become granule cells by P19 (Fig. 1b). Notably, the newly generated granule cells labeled by GFP (Supplementary Fig. 3) or BrdU (Namba et al. 2005) at P5 were distributed evenly in the GCL at P19, suggesting that these neurons contribute to establish the GCL with uniform depth. In the following analysis, we focused on the GFP+Hu+ neurons in the hilus at P8 because these cells are likely to be migrating immature granule cells.

This assumption is further corroborated by the following findings; (i) most of the GFP+Hu+ neurons in the hilus at P8 also expressed a granule cell marker Prox1 (89.7% ± 4, total 81 cells were counted, (Supplementary Fig. 2b)), but (ii) none of them expressed interneuron markers GABA (Supplementary Fig. 2c) nor calretinin (Supplementary Fig. 2d; note that calretinin is expressed also in immature granule cells in mouse but only in the subset of interneurons in rat (Murakawa and Kosaka 1999)). (iii) None of microglial cells identified by Iba-1 expressed Hu in the hilus at P8 (Supplementary Fig. 1e).

Embryonic neocortical neurons tend to extend a relatively thick leading process in the direction of movement (toward the cortical plate) and then translocate the nuclei into the leading process. The neurons repeat this cycle during migration (Kawauchi 2015; Nadarajah et al. 2003; Namba et al. 2015; Reiner and Sapir 2013). Therefore, leading process orientation may allow us to predict the direction of initial cell movement in the DG. We categorized the morphology and the directionality of GFP+Hu+ cells (excluding cells formed a cluster and/or with faint GFP signal) in the hilus into three types: (1) uni-directional bipolar cells, which possess both a relatively thick leading process and a thin trailing process (Fig. 1c, 59.4% ± 1.7), (2) bi-directional cells, bipolar cells with two processes of similar thickness (Fig. 1c, 16.0% ± 0.7), and (3) multipolar cells with multiple short processes (Fig. 1c, 24.5% ± 2.3) (as previously described in the neonatal DG (Namba et al. 2005) that have similar features observed in the developmental neocortex (Jossin and Cooper 2011; Namba et al. 2014; Tabata and Nakajima 2003)). These results were corroborated by the analysis focused on the Prox1-expressing GFP+Hu+ cells (Supplementary Fig. 2b).

We next examined whether the leading processes of uni-directional bipolar cells oriented toward the GCL, the final destination of migrating immature granule neurons. We plotted GFP+Hu+ uni-directional bipolar cells in the hilus according to their location and the orientation of their leading processes (Fig. 1d). The uni-directional bipolar cells were distributed throughout the hilus. The majority of GFP+Hu+ cells in the hilus were found to orient the leading process at an angle of a range from 45° to 135° to the shortest path to the GCL (Fig. 1d, e). This result indicates that most uni-directional cells did not orient towards the closest part of the GCL, suggesting that the direction of their initial movement is not toward the GCL. Although previous studies have suggested that most or all immature granule neurons migrate radially toward the GCL (Nakahira and Yuasa 2005; Rickmann et al. 1987), our cell orientation measurements raise the possibility that tangential migration also contributes to the generation of the U-shaped GCL.

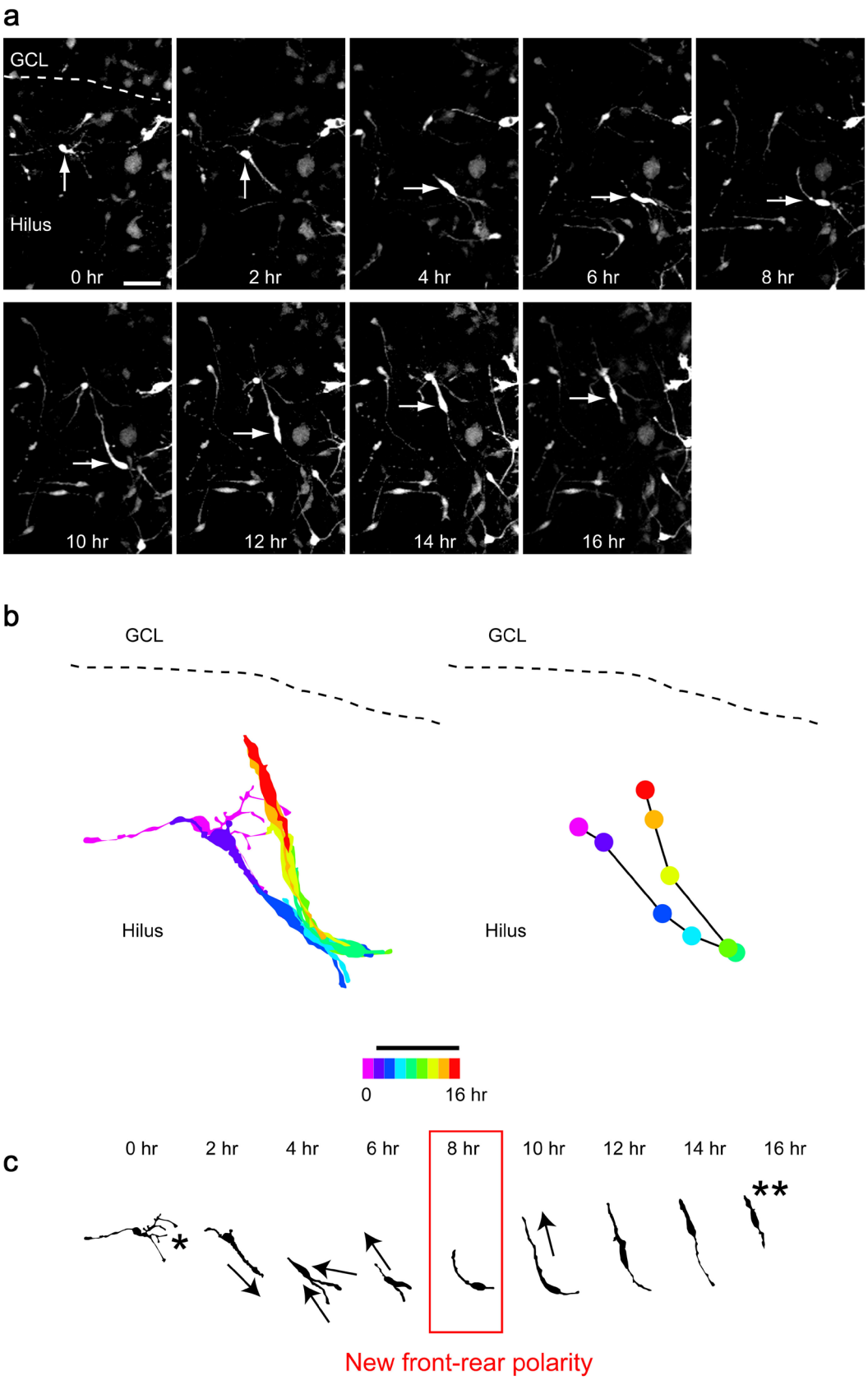
a
GCL
Hilus
0 hr
2 hr
4 hr
6 hr
8 hr
10 hr
12 hr
14 hr
16 hr
b
GCL
GCL
Hilus
Hilus
0
16 hr
c
0 hr
2 hr
4 hr
6 hr
8 hr
10 hr
12 hr
14 hr
16 hr
*
**
New front-rear polarity

◂**Fig. 4** Time-lapse images of turning the movement of a GFP+cell that showed 180° turning during the migration. Retrovirus carrying GFP was injected into DG at P5. Time-lapse imaging was started at P8. Images were taken every 2 h. **a** Still images of GFP+cells that changed their direction during migration. Scale bar, 50 µm. **b**, **c** Outline of the cell indicated by arrows in (**a**). **b** Trajectory of the cell (left) and position of cell soma (right) over time. Black line in the right panel shows the trajectory of soma. Each time-point is color-coded in the bottom of the panel. Scale bar, 50 µm. **c** Morphological changes of the cell over time. Asterisk indicates the initial leading processes. Double asterisk indicates the new leading processes. Small arrows indicate the neurite extension and retraction. Red box indicates the time point in which the cell established new front–rear polarity

Radial and non-radial migrations of newly generated neurons

Because the cell orientation measurements only predict the initial direction of the neuronal migration but cannot predict the migratory behavior afterwards, the migratory behavior of newborn granule cells needs to be observed directly by organotypic slice culture together with time-lapse imaging (Namba et al. 2007, 2011b). We previously demonstrated that there are no significant differences in the final localization of postnatally generated granule neurons between cultured and in vivo conditions (Namba et al. 2007), suggesting that neuronal migration in culture largely recapitulates normal neuronal migration from the hilus to the GCL. We stereotaxically injected retroviral vector into the rat DG at P5 and prepared hippocampal slice cultures 3 days later (at P8), when a sufficiently robust GFP signal was present. Confocal images were then collected in 2 h intervals to generate a time-lapse of neuronal migration.

We focused on the uni- and bi-directional cells because these cellular morphotypes represent the majority of migrating neurons as described above. All uni-directional bipolar cells initially moved toward the direction of the leading process, confirming that the assumption of the leading process orientation measurement is correct. Notably, time-lapse imaging revealed that multipolar cells in the hilus transformed into bipolar cells Supplementary Fig. 4), as previously described for migrating neocortical neurons (Barnes and Polleux 2009; Namba et al. 2015; Tahirovic and Bradke 2009).We did not analyze the GFP+ mitotic cells to exclude progenitor cells from the present analysis (Supplementary Fig. 5). Because the cell cycle length of the progenitor cells in the postnatal dentate gyrus was calculated as approximately 15–16 h (Nowakowski et al. 1989; Varodayan et al. 2009), the GFP+ cells without showing a cell division at least in 20 h of imaging were most likely postmitotic cells.

48.75% of imaged cells migrated directly toward the GCL without directional changes, that is, they migrated radially (Figs. 2a, b, 6a). These cells migrated in the range between 45° and −45° from their initial directions at the start of imaging (0°) (Fig. 6b). In contrast, the remaining cells turned 2.9 times on average within the first 24 h of imaging (Figs. 3, 4, 5). These cells turned greater than 45° from their starting directions (0°) (Fig. 6c), suggesting that cells in this population migrate laterally or even reverse direction entirely. We observed that the leading processes of non-radially migrating cells often retracted, elongated de novo, or formed collateral branches (Figs. 3, 4, 5), indicating that their leading processes are less stable compared with those of cells with strict radial migration (Fig. 2). The average migration distance of cell soma per hour was slightly different between cells without directional changes and cells with directional changes (6.5 µm ± 0.7 and 5.4 µm ± 0.8, respectively; $n = 20$ cells in each group).

We next analyzed the morphological changes of GFP+ cells undergoing directional reorientation. Migrating neurons can change direction by three modes based upon the subcellular regions where process formation or process transformation occur (Fig. 6d). The first mode is through the formation of a new neurite from the soma (at 4 h, Fig. 3a, c) (mode #1, turning). The de novo neurite becomes a leading process and a new trailing process arises from the opposite site; the initial leading process can be retracted either before or after the new leading process develops.

The second mode of directional change is through the transformation of the trailing process into the leading process (at 8 h, Fig. 4a, c) (mode #2, 180° turning). The trailing process becomes thicker as the leading process thins. The thickness of both processes is almost equal halfway through the process of reorientation. The bi-directional cells described above might, therefore, represent a transient state of mode #2. The third mode involves collateral formation from the initial leading process (at 2 h, Fig. 5a, c) (mode #3, veering). In this case, the collateral becomes thick and finally develops into a main leading process (at 12 h, Fig. 5a, c).

Finally, we determined the relative frequencies of these three modes of reorientation for newborn granule cells migrating to the GCL (Fig. 6e). The most frequent way to change direction is through mode #1 (36.8%). The occurrences of modes #2 and #3 are approximately equal (18.4% and 15.8%, respectively). The remaining 28.9% of imaged cells underwent sequential directional changes through combinations of modes #1, #2 and #3. Our results demonstrate that newly generated neurons of the neonatal DG migrate not only by the conventional radial mode but also by at least three non-radial modes that disperse immature neurons along the developing GCL.

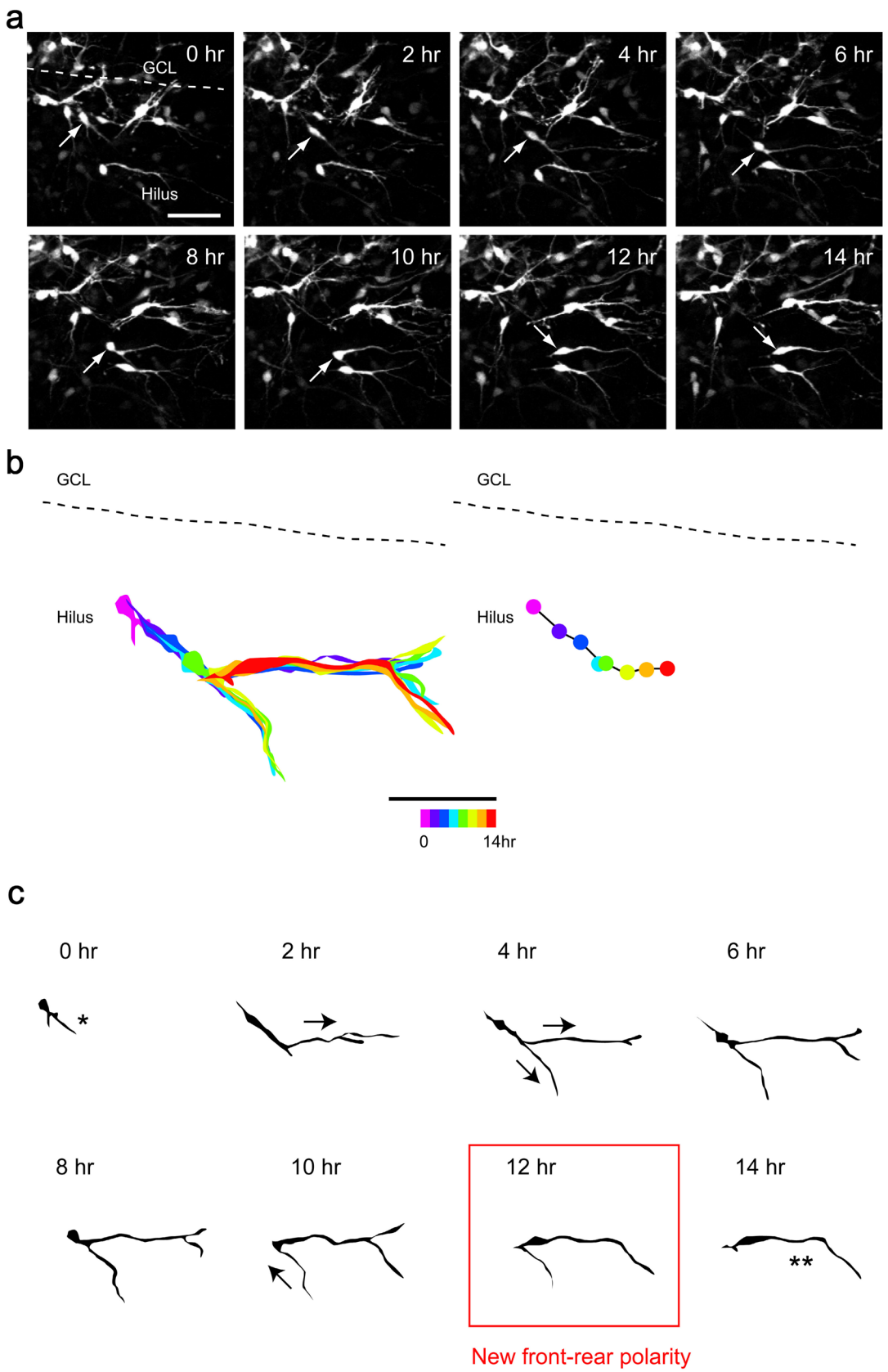
a
0 hr
GCL
Hilus
2 hr
4 hr
6 hr
8 hr
10 hr
12 hr
14 hr
b
GCL
GCL
Hilus
Hilus
0
14hr
c
0 hr
2 hr
4 hr
6 hr
8 hr
10 hr
12 hr
14 hr
New front-rear polarity

◂**Fig. 5** Time-lapse images of a GFP+ cell that showed a collateral formation from the leading process during the migration. Retrovirus carrying GFP was injected into DG at P5. Time-lapse imaging was started at P8. Images were taken every 2 h. **a** Still images of GFP+ cells that changed their direction during migration. The outline of cell indicated by arrows is shown in (**b**) and (**c**). Scale bar, 50 µm. b, c Outline of the cell indicated by arrows in (**a**). (**b**) Trajectory of the cell (left) and the position of cell soma (right) over time. Black line in the right panel shows the trajectory of soma. Each timepoint is color-coded in the bottom of the panel. Scale bar, 50 µm. **c** Morphological changes of the cell over time. Asterisk indicates the initial leading processes. Double asterisk indicates the new leading processes. Small arrows indicate the neurite extension and retraction. Red box indicates the time point in which the cell established new front–rear polarity

Discussion

In the postnatal hilus, new neurons are continuously generated and migrate to the GCL where they contribute to hippocampal circuitry. The present immunohistochemical and time-lapse imaging analyses demonstrate that the postnatally generated neurons in the hilus exhibit both radial and non-radial migrations, in roughly equal proportions, and during non-radial migration they change the direction of migration with turning and veering movements. During early postnatal development, the dentate GCL acquires a U-shaped morphology with a densely packed cell layer of uniform depth. Our data raise the interesting possibility that intricate tangential migration modes serve to distribute granule neurons evenly throughout the GCL and contribute to its mature U-shaped architecture.

Radial migration

Our time-lapse imaging experiments revealed that half of new neurons migrate radially to the GCL without turning or veering (Fig. 6). Radial migration of immature neurons has been well-studied in the embryonic neocortex, where pyramidal neurons born in the VZ and SVZ migrate to the cortical plate along radial glial cell processes (Barnes and Polleux 2009; Namba et al. 2015; Tahirovic and Bradke 2009). The radial migrations described in the embryonic rodent neocortex (see below about the ferret neocortex) and in the postnatal rodent hilus share some features. In both cases, migrating bipolar neurons are spindle-shaped cells with a thick leading process extending in the direction of migration as well as a thin trailing process. Moreover, in both regions, subset of bipolar neurons migrates toward the pial surface of the brain (or towards the hippocampal fissure) in a relatively straight path.

Consistent with our data, one previous study demonstrated that newborn granule cells labeled by in utero electroporation of a GFP expression vector migrated radially towards the GCL along radial glial fibers (Nakahira and Yuasa 2005). Additionally, another group recently reported that the radial migration is observed in the subset of transgenically labeled granule neurons in hippocampus slice culture obtained from proopiomelanocortin (POMC)-EGFP transgenic mice (Wang et al. 2018). In this transgenic mouse, a majority of immature POMC-EGFP+ neurons appear to be located in the GCL and proximal to the GCL, but not deeply within the hilus (Wang et al. 2018). In contrast, our retrovirus-labeling experiments labeled progenitor cells in the entire hilus relatively evenly and revealed a novel population of tangentially migrating neurons in addition to the previously described radial migrations.

Non-radial tortuous migration

In the present study, we found that half of the uni-directional bipolar cells did not orient directly toward the nearest part of the GCL. These data suggest that many newborn granule neurons do not minimize their distance of travel to the GCL but instead migrate tangentially through the hilus before reaching a more distant location. Additionally, newly generated neurons in the postnatal hilus adopted at least two additional morphologies: bi-directional cells and multipolar cells. We suggest that the bi-directional cells represent a transient state of 180° turning at which the thickening trailing process and thinning leading process are of approximately equal diameter (Fig. 4) (Gertz and Kriegstein 2015; Nadarajah et al. 2002). The multipolar cells were observed to migrate short distances, unlike bipolar cells (Hatanaka and Yamauchi 2013; Namba et al. 2014; Sakakibara et al. 2014; Tabata and Nakajima 2003).

Further supporting our immunohistochemical analysis, time-lapse imaging of uni- and bi-directional cells demonstrated several distinct modes of non-radial migration accompanied by veering and turning. Furthermore, analysis of leading processes of migrating newborn neurons revealed their continuous branching and leading-to-trailing transformation, changes that are reported to be involved in non-radial migrations (Gertz and Kriegstein 2015; Nadarajah et al. 2002; Valiente and Martini 2009). These findings, together with the previous findings in the subgranular region (Seki et al. 2007; Wang et al. 2018), lead us to hypothesize that the non-radial migration might contribute to the lateral dispersion of granule neurons, and thus constructing the U-shaped GCL.

This hypothesis is supported by previous reports showing that the non-radial migration disperse newly generated neurons in the developing neocortex (Gertz and Kriegstein 2015; Martinez-Martinez et al. 2018; Tanaka et al. 2009). For example, inhibitory interneurons derived from the ganglionic eminences migrate tangentially in the intermediate zone and, after reaching the developing neocortex, exhibit multidirectional movements in the marginal zone (Tanaka

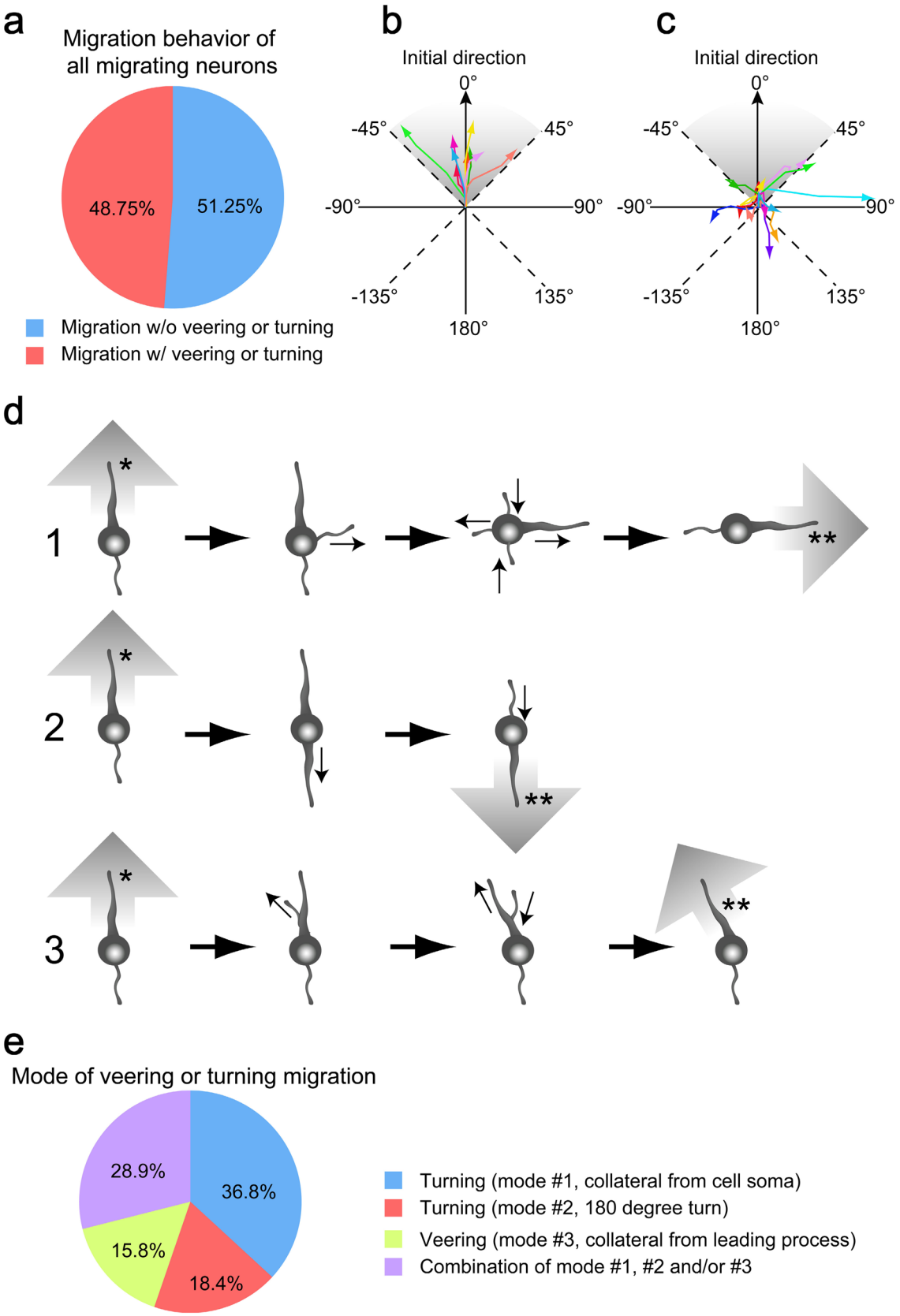
a
Migration behavior of all migrating neurons
48.75%
51.25%
Migration w/o veering or turning
Migration w/ veering or turning
b
Initial direction
0°
-45°
45°
-90°
90°
-135°
135°
180°
c
Initial direction
0°
-45°
45°
-90°
90°
-135°
135°
180°
d
1
2
3
*
**
e
Mode of veering or turning migration
28.9%
36.8%
15.8%
18.4%
Turning (mode #1, collateral from cell soma)
Turning (mode #2, 180 degree turn)
Veering (mode #3, collateral from leading process)
Combination of mode #1, #2 and/or #3

◂**Fig. 6** Quantification of GFP+cell migration observed by a time-lapse imaging. **a** Quantification of the percentage of GFP+migrating cells with (red) or without (blue) veering or turning. Total 80 cells from four independent experiments (7–12 slices per experiment) were analyzed. **b**, **c** Trace of the GFP+cell trajectories without (**b**) and with (**c**) veering or turning. Zero degree represents the initial direction of cells. Arrows with different colors indicate the trajectories of each GFP+cells. **d** Schematic diagram of neurite formation. Mode #1: collateral formation from cell soma; mode #2: 180° turning; mode #3: collateral formation from the initial leading process. Asterisks indicate the initial leading processes. Double asterisks indicate the new leading processes. Small black arrows indicate the neurite extension and retraction. Big gray arrows indicate the direction of migration. **e** Quantification of the percentage of GFP+migrating neurons that exhibit different modes of veering and/or turning as described in (**d**). Total 38 cells from 4 independent experiments (7–12 slices per experiment) were analyzed

et al. 2009). This multidirectional migration is thought to spread interneurons evenly across neocortical areas and layers.

Other examples of non-radial migration are found in the developing ferret neocortex, which unlike the mouse neocortex is gyrencephalic (Gertz and Kriegstein 2015; Martinez-Martinez et al. 2018). Immature neocortical pyramidal neurons begin to migrate tortuously with turning and veering following the onset of gyrification, suggesting a relationship between tortuous migration of neurons and the formation of neocortical folds. Because neuronal clones are more widely dispersed in the gyrencephalic ferret neocortex than in the lissencephalic rodent neocortex (Kornack and Rakic 1995; Reid et al. 1997; Ware et al. 1999), tortuous migration is thought to be involved in the lateral dispersion of neurons and the formation of the sectoral-shaped neocortical columns (Gertz and Kriegstein 2015; Martinez-Martinez et al. 2018). Therefore, by analogy with the formation of a folded neocortical sheet, tortuous migration in the postnatal DG may be beneficial to the lateral dispersion of neurons.

Why hippocampal granule cells migrate tortuously is an issue to be addressed. One possibility is that the lateral dispersion of neurons may allow migrating neurons to find a space to be integrated. The other possibility is that migrating neurons may be searching external cues (e.g., the radial process of the basal radial glia-like cells (Supplementary Fig. 5); see below) to be established the axon-dendrite polarity and/or to determine their direction.

Process formation and cell polarity

Our time-lapse observations revealed that turning is accompanied by process formation that is thought to be closely associated with changes to cell polarity (Barnes and Polleux 2009; Namba et al. 2015; Tahirovic and Bradke 2009). There are two principal types of cell polarity in neurons. Front-rear polarity is required for a proper neuronal migration during development, whereas axon–dendrite polarity governs the identity of mature neuronal processes. Generally, migrating neurons extend a leading process and a trailing process. Because neurons extend the leading process in the direction of movement, the leading process and the trailing process are defined as front and rear, respectively. The leading process and the trailing process of mouse embryonic neocortical neurons eventually give rise to the dendrites and axon, respectively. Thus, the eventual axon–dendrite polarity of differentiated neurons is established early in development with the onset of front–rear polarity and neuronal migration (Hatanaka and Yamauchi 2013; Namba et al. 2014; Sakakibara et al. 2014).

In the present study, we described postnatal hippocampal granule neurons migrate with retraction and de novo extension of the leading process (mode #1 and/or mode #2 Fig. 6e). The repeated process formation suggests that these neurons have a relatively plastic front–rear polarity, but have not yet committed to a final axon–dendrite polarity. Therefore, in contrast to the mouse embryonic neocortical neurons, at least 40% of rat hippocampal granule neurons may undergo polarization sequentially, first front–rear and then axon–dendrite (calculated from Fig. 6a and Fig. 6e; 84.2% of the total migrating neurons with veering or turning).

Future directions

As postnatal development proceeds, the neurogenic area of the hilus diminishes and becomes confined to the sub granular zone (SGZ) (Altman and Bayer 1990a; Matsue et al. 2018; Namba et al. 2005; Nicola et al. 2015; Seki et al. 2014). In the adult SGZ, neuronal progenitors proliferate and then form clusters of progenitors and immature neurons. New neurons then likely distribute to surrounding regions by tangential migration (Seki et al. 2007), suggesting that non-radial migration is important for uniform distribution of newly generated neurons in both the postnatal and adult GCL.

The mechanisms that dictate whether newborn granule neurons undergo radial or tangential migration need to be addressed. One possibility is that immature neurons derived from different subtype of progenitor cells (e.g., intermediate progenitor cells that lack the radial process (Namba et al. 2011b) vs. basal/outer radial glia-like cells that possess a radial process (LaMonica et al. 2012; Namba and Huttner 2017; Namba et al. 2005, 2011b; Rickmann et al. 1987; Sievers et al. 1992)) exhibit different migratory behavior. The probability of the contact to the radial process might be higher in the neurons derived from the basal/outer radial glia-like cells than the neurons generated from the intermediate progenitor cells, thus the neurons can utilize the radial process for their migration.

The relationship between the progenitor cell subtypes and migratory behavior of neurons needs further studies.

The other possibility is that the migratory behaviors are controlled by some combination of mechanisms intrinsic to migrating granule neurons, environmental cues encountered during migration. The intrinsic polarity proteins and extrinsic microenvironmental factors such as extracellular matrix and cell–cell interaction are known to be involved in neuronal polarization and migration in the neocortex (reviewed in (Barnes and Polleux 2009; Cooper 2014; Funahashi et al. 2014; Namba et al. 2015)). Neurotransmitters have been shown to regulate neuronal migration in the DG (Koyama et al. 2012; Namba et al. 2011a). Notably, fibril seizures induced by hyperthermic conditions are reported to change the direction of granule cell migration through upregulation of $GABA_A$ receptors in postnatal rats (Koyama et al. 2012).

Our present study provides a new model for understanding the intrinsic and extrinsic regulatory mechanisms underlying the proper distribution of new neurons by non-radial migratory behavior.

Acknowledgements We very thank Drs Hirotaka J. Okano (Keio University) and Robert B. Darnell (The Rockefeller University) for anti-Hu antibody, Nobuaki Tamamaki (Kumamoto University) for the anti-GFP antibody and Hideki Mochizuki (Osaka University) for the retroviral vector. We also thank Dr. Hideo Namiki (Waseda University) for the generous support of this study. We appreciate the review of the manuscript and useful comments on it by Dr. Steven D. Briscoe (Max Planck Institute of Molecular Cell Biology and Genetics).

Author contributions Conceptualization, TN and TS; formal analysis, TN; investigation, TN and HS; writing—original draft, TN, with input from TS; writing—review and editing, TN and TS; supervision, TS; project administration and funding acquisition, TS.

Funding TS is supported by JSPS (22500306).

Compliance with ethical standards

Conflict of interest The authors declare no competing interests.

Research involving human participants and/or animals All animal experiments were approved by the institutional animal care and use committee at Juntendo University and Tokyo Medical University.

Informed consent All experiments were performed on rats.

References

Abrous DN, Wojtowicz JM (2015) Interaction between neurogenesis and hippocampal memory system: new vistas. Cold Spring Harb Perspect Biol. https://doi.org/10.1101/cshperspect.a018952

Altman J, Bayer SA (1990a) Migration and distribution of two populations of hippocampal granule cell precursors during the perinatal and postnatal periods. J Comp Neurol 301:365–381

Altman J, Bayer SA (1990b) Mosaic organization of the hippocampal neuroepithelium and the multiple germinal sources of dentate granule cells. J Comp Neurol 301:325–342

Altman J, Das GD (1965) Post-natal origin of microneurones in the rat brain. Nature 207:953–956

Amaral DG, Dent JA (1981) Development of the mossy fibers of the dentate gyrus: I. A light and electron microscopic study of the mossy fibers and their expansions. J Comp Neurol 195:51–86. https://doi.org/10.1002/cne.901950106

Barnes AP, Polleux F (2009) Establishment of axon–dendrite polarity in developing neurons. Annu Rev Neurosci 32:347–381. https://doi.org/10.1146/annurev.neuro.31.060407.125536

Bayer SA (1980) Development of the hippocampal region in the rat. I. Neurogenesis examined with 3H-thymidine autoradiography. J Comp Neurol 190:87–114

Bayer SA, Altman J (1975) Radiation-induced interference with postnatal hippocampal cytogenesis in rats and its long-term effects on the acquisition of neurons and glia. J Comp Neurol 163:1–19. https://doi.org/10.1002/cne.901630102

Blaabjerg M, Zimmer J (2007) The dentate mossy fibers: structural organization, development and plasticity. Prog Brain Res 163:85–107. https://doi.org/10.1016/S0079-6123(07)63005-2

Cooper JA (2014) Molecules and mechanisms that regulate multipolar migration in the intermediate zone. Front Cell Neurosci 8:386. https://doi.org/10.3389/fncel.2014.00386

Eriksson PS, Perfilieva E, Bjork-Eriksson T, Alborn AM, Nordborg C, Peterson DA, Gage FH (1998) Neurogenesis in the adult human hippocampus. Nat Med 4:1313–1317. https://doi.org/10.1038/3305

Funahashi Y, Namba T, Nakamuta S, Kaibuchi K (2014) Neuronal polarization in vivo: growing in a complex environment. Curr Opin Neurobiol 27:215–223. https://doi.org/10.1016/j.conb.2014.04.009

Gertz CC, Kriegstein AR (2015) Neuronal migration dynamics in the developing ferret cortex. J Neurosci 35:14307–14315. https://doi.org/10.1523/JNEUROSCI.2198-15.2015

Hatanaka Y, Yamauchi K (2013) Excitatory cortical neurons with multipolar shape establish neuronal polarity by forming a tangentially oriented axon in the intermediate zone. Cereb Cortex 23:105–113. https://doi.org/10.1093/cercor/bhr383

Hevner RF (2016) Evolution of the mammalian dentate gyrus. J Comp Neurol 524:578–594. https://doi.org/10.1002/cne.23851

Josselyn SA, Kohler S, Frankland PW (2015) Finding the engram. Nat Rev Neurosci 16:521–534. https://doi.org/10.1038/nrn4000

Jossin Y, Cooper JA (2011) Reelin, Rap1 and N-cadherin orient the migration of multipolar neurons in the developing neocortex. Nat Neurosci 14:697–703. https://doi.org/10.1038/nn.2816

Kawauchi T (2015) Cellullar insights into cerebral cortical development: focusing on the locomotion mode of neuronal migration. Front Cell Neurosci 9:394. https://doi.org/10.3389/fncel.2015.00394

Kempermann G (2019) Environmental enrichment, new neurons and the neurobiology of individuality. Nat Rev Neurosci 20:235–245. https://doi.org/10.1038/s41583-019-0120-x

Kerjan G, Gleeson JG (2007) Genetic mechanisms underlying abnormal neuronal migration in classical lissencephaly. Trends Genet TIG 23:623–630. https://doi.org/10.1016/j.tig.2007.09.003

Kornack DR, Rakic P (1995) Radial and horizontal deployment of clonally related cells in the primate neocortex: relationship to distinct mitotic lineages. Neuron 15:311–321

Koyama R et al (2012) GABAergic excitation after febrile seizures induces ectopic granule cells and adult epilepsy. Nat Med 18:1271–1278. https://doi.org/10.1038/nm.2850

Kuhn HG, Dickinson-Anson H, Gage FH (1996) Neurogenesis in the dentate gyrus of the adult rat: age-related decrease of neuronal progenitor proliferation. J Neurosci 16:2027–2033

LaMonica BE, Lui JH, Wang X, Kriegstein AR (2012) OSVZ progenitors in the human cortex: an updated perspective on neurodevelopmental disease. Curr Opin Neurobiol 22:747–753. https://doi.org/10.1016/j.conb.2012.03.006

Li G, Pleasure SJ (2014) The development of hippocampal cellular assemblies Wiley interdisciplinary reviews. Dev Biol 3:165–177. https://doi.org/10.1002/wdev.127

Martinez-Martinez MA, Ciceri G, Espinos A, Fernandez V, Marin O, Borrell V (2018) Extensive branching of radially-migrating neurons in the mammalian cerebral cortex. J Comp Neurol. https://doi.org/10.1002/cne.24597

Matsue K, Minakawa S, Kashiwagi T, Toda K, Sato T, Shioda S, Seki T (2018) Dentate granule progenitor cell properties are rapidly altered soon after birth. Brain Struct Funct 223:357–369. https://doi.org/10.1007/s00429-017-1499-7

Moser EI, Moser MB, McNaughton BL (2017) Spatial representation in the hippocampal formation: a history. Nat Neurosci 20:1448–1464. https://doi.org/10.1038/nn.4653

Murakawa R, Kosaka T (1999) Diversity of the calretinin immunoreactivity in the dentate gyrus of gerbils, hamsters, guinea pigs, and laboratory shrews. J Comp Neurol 411:413–430

Nadarajah B, Alifragis P, Wong RO, Parnavelas JG (2002) Ventricle-directed migration in the developing cerebral cortex. Nat Neurosci 5:218–224

Nadarajah B, Alifragis P, Wong RO, Parnavelas JG (2003) Neuronal migration in the developing cerebral cortex: observations based on real-time imaging. Cereb Cortex 13:607–611

Nakahira E, Yuasa S (2005) Neuronal generation, migration, and differentiation in the mouse hippocampal primoridium as revealed by enhanced green fluorescent protein gene transfer by means of in utero electroporation. J Comp Neurol 483:329–340

Nakazawa K, McHugh TJ, Wilson MA, Tonegawa S (2004) NMDA receptors, place cells and hippocampal spatial memory. Nat Rev Neurosci 5:361–372. https://doi.org/10.1038/nrn1385

Namba T, Huttner WB (2017) Neural progenitor cells and their role in the development and evolutionary expansion of the neocortex. WIREs Dev Biol 6:e256. https://doi.org/10.1002/wdev.256

Namba T, Mochizuki H, Onodera M, Mizuno Y, Namiki H, Seki T (2005) The fate of neural progenitor cells expressing astrocytic and radial glial markers in the postnatal rat dentate gyrus. Eur J Neurosci 22:1928–1941. https://doi.org/10.1111/j.1460-9568.2005.04396.x

Namba T, Mochizuki H, Onodera M, Namiki H, Seki T (2007) Postnatal neurogenesis in hippocampal slice cultures: early in vitro labeling of neural precursor cells leads to efficient neuronal production. J Neurosci Res 85:1704–1712

Namba T et al (2011a) NMDA receptor regulates migration of newly generated neurons in the adult hippocampus via disrupted-in-schizophrenia 1 (DISC1). J Neurochem 118:34–44. https://doi.org/10.1111/j.1471-4159.2011.07282.x

Namba T et al (2011b) Time-lapse imaging reveals symmetric neurogenic cell division of GFAP-expressing progenitors for expansion of postnatal dentate granule neurons. PLoS One 6:e25303. https://doi.org/10.1371/journal.pone.0025303

Namba T et al (2014) Pioneering axons regulate neuronal polarization in the developing cerebral cortex. Neuron 81:814–829. https://doi.org/10.1016/j.neuron.2013.12.015

Namba T, Funahashi Y, Nakamuta S, Xu C, Takano T, Kaibuchi K (2015) Extracellular and intracellular signaling for neuronal polarity. Physiol Rev 95:995–1024. https://doi.org/10.1152/physrev.00025.2014

Nicola Z, Fabel K, Kempermann G (2015) Development of the adult neurogenic niche in the hippocampus of mice. Front Neuroanat 9:53. https://doi.org/10.3389/fnana.2015.00053

Noctor SC, Flint AC, Weissman TA, Dammerman RS, Kriegstein AR (2001) Neurons derived from radial glial cells establish radial units in neocortex. Nature 409:714–720

Nowakowski RS, Rakic P (1981) The site of origin and route and rate of migration of neurons to the hippocampal region of the rhesus monkey. J Comp Neurol 196:129–154. https://doi.org/10.1002/cne.901960110

Nowakowski RS, Lewin SB, Miller MW (1989) Bromodeoxyuridine immunohistochemical determination of the lengths of the cell cycle and the DNA-synthetic phase for an anatomically defined population. J Neurocytol 18:311–318

Rakic P, Nowakowski RS (1981) The time of origin of neurons in the hippocampal region of the rhesus monkey. J Comp Neurol 196:99–128. https://doi.org/10.1002/cne.901960109

Reid CB, Tavazoie SF, Walsh CA (1997) Clonal dispersion and evidence for asymmetric cell division in ferret cortex. Development 124:2441–2450

Reiner O, Sapir T (2013) LIS1 functions in normal development and disease. Curr Opin Neurobiol 23:951–956. https://doi.org/10.1016/j.conb.2013.08.001

Rickmann M, Amaral DG, Cowan WM (1987) Organization of radial glial cells during the development of the rat dentate gyrus. J Comp Neurol 264:449–479

Sakakibara A, Sato T, Ando R, Noguchi N, Masaoka M, Miyata T (2014) Dynamics of centrosome translocation and microtubule organization in neocortical neurons during distinct modes of polarization. Cereb Cortex 24:1301–1310. https://doi.org/10.1093/cercor/bhs411

Schlessinger AR, Cowan WM, Gottlieb DI (1975) An autoradiographic study of the time of origin and the pattern of granule cell migration in the dentate gyrus of the rat. J Comp Neurol 159:149–175

Seki T, Arai Y (1993) Highly polysialylated neural cell adhesion molecule (NCAM-H) is expressed by newly generated granule cells in the dentate gyrus of the adult rat. J Neurosci 13:2351–2358

Seki T, Arai Y (1995) Age-related production of new granule cells in the adult dentate gyrus. NeuroReport 6:2479–2482

Seki T, Namba T, Mochizuki H, Onodera M (2007) Clustering, migration, and neurite formation of neural precursor cells in the adult rat hippocampus. J Comp Neurol 502:275–290. https://doi.org/10.1002/cne.21301

Seki T, Sato T, Toda K, Osumi N, Imura T, Shioda S (2014) Distinctive population of Gfap-expressing neural progenitors arising around the dentate notch migrate and form the granule cell layer in the developing hippocampus. J Comp Neurol 522:261–283. https://doi.org/10.1002/cne.23460

Sievers J, Hartmann D, Pehlemann FW, Berry M (1992) Development of astroglial cells in the proliferative matrices, the granule cell layer, and the hippocampal fissure of the hamster dentate gyrus. J Comp Neurol 320:1–32

Stouffer MA, Golden JA, Francis F (2016) Neuronal migration disorders: focus on the cytoskeleton and epilepsy. Neurobiol Dis 92:18–45. https://doi.org/10.1016/j.nbd.2015.08.003

Suzuki A et al (2002) Feasibility of ex vivo gene therapy for neurological disorders using the new retroviral vector GCDNsap packaged in the vesicular stomatitis virus G protein. J Neurochem 82:953–960

Tabata H, Nakajima K (2003) Multipolar migration: the third mode of radial neuronal migration in the developing cerebral cortex. J Neurosci 23:9996–10001

Tahirovic S, Bradke F (2009) Neuronal polarity. Cold Spring Harb Perspect Biol 1:a001644. https://doi.org/10.1101/cshperspect.a001644

Tanaka DH et al (2009) Random walk behavior of migrating cortical interneurons in the marginal zone: time-lapse analysis

in flat-mount cortex. J Neurosci 29:1300–1311. https://doi.org/10.1523/JNEUROSCI.5446-08.2009

Toda T, Gage FH (2018) Review: adult neurogenesis contributes to hippocampal plasticity. Cell Tissue Res 373:693–709. https://doi.org/10.1007/s00441-017-2735-4

Valiente M, Martini FJ (2009) Migration of cortical interneurons relies on branched leading process dynamics. Cell Adhes Migr 3:278–280

Varodayan FP, Zhu XJ, Cui XN, Porter BE (2009) Seizures increase cell proliferation in the dentate gyrus by shortening progenitor cell-cycle length. Epilepsia 50:2638–2647. https://doi.org/10.1111/j.1528-1167.2009.02244.x

Wang S et al (2018) Trajectory analysis unveils Reelin's role in the directed migration of granule cells in the dentate gyrus. J Neurosci 38:137–148. https://doi.org/10.1523/JNEUROSCI.0988-17.2017

Ware ML, Tavazoie SF, Reid CB, Walsh CA (1999) Coexistence of widespread clones and large radial clones in early embryonic ferret cortex. Cereb Cortex 9:636–645